

Optical intensity mapping on the nanometer scale by near-field photodetection optical microscopy

R. C. Davis and C. C. Williams

Department of Physics, University of Utah, Salt Lake City, Utah 84112

P. Neuzil

Microfabrication Applications Laboratory, University of Illinois at Chicago, Chicago, Illinois 60607

Received September 14, 1995

Near-field photodetection optical microscopy (NPOM) is a fundamentally new approach to near-field optical microscopy. This scanning-probe technique uses a nanometer-scale photodiode detector as a near-field optical probe. We have fabricated probes for NPOM that have optically sensitive areas as small as $100\text{ nm} \times 100\text{ nm}$. These new NPOM probes have been employed to image light transmitted through holes in an aluminum film. Near-surface optical interference is observed near defects and edges of the aluminum film. The optical edge response is shown to be of the order of 100 nm . © 1996 Optical Society of America

Optical measurements with nanometer-scale resolution are now possible with optical scanning-probe microscopy techniques.¹⁻⁴ Near-field photodetection optical microscopy⁵⁻⁹ (NPOM) is a new fundamentally different approach to near-field optical microscopy that utilizes a photodetector of subwavelength dimensions. In standard near-field scanning optical microscopy light is scattered through an aperture and collected with a detector in the far field. In contrast, NPOM utilizes a localized scanning photodetector probe that is brought into the optical near field of an illuminated surface where it can directly absorb optical power. As it is raster scanned across the surface, the photocurrent signal is recorded to create a two-dimensional image of the optical intensity distribution. A small detector is necessary for high spatial resolution. Recently local photodetectors and light sources were constructed.⁵⁻¹⁰ In a previous paper we reported batch fabricating probes for NPOM with $500\text{ nm} \times 500\text{ nm}$ optically sensitive areas.⁹ Here we present a significant improvement on previous photodetectors, resulting in probes that have optically sensitive areas as small as $100\text{ nm} \times 100\text{ nm}$. We believe that the results presented here represent the first two-dimensional near-field imaging with a subwavelength photodetector probe ($100\text{ nm} \times 100\text{ nm}$) yielding spatial resolution on the 100-nm scale. Near-surface optical interference is also observed near defects and edges of an aluminum film.

The basic fabrication process for the silicon photodiode probes is described in detail elsewhere.⁹ The photodiodes are constructed on oxidized pyramidal silicon tips based on the following process: Photoresist is spun on the entire wafer and is found to pull back the sharp region near the end of the tips owing to surface forces. Using the photoresist process and an etch step, we remove the silicon dioxide from a $2\text{-}\mu\text{m}$ region near the end of the tips by using the resist as a mask. Aluminum is then deposited over the entire structure. Using the photoresist process a second time with an aluminum etch, we remove a small region of aluminum, approximately 100 nm , exposing the silicon at the end of the tips.

Figure 1 (bottom) is a cut-away schematic of the probe structure showing a micromachined silicon pyramid with 100-nm silicon dioxide covering all but the last $2\text{ }\mu\text{m}$ of the tip. This structure is covered with an 80-nm aluminum film with a small opening ($100\text{--}200\text{ nm}$) in the film at the end of the tip. Scanning-electron-microscopy images of the resultant nanoprobe are shown in Fig. 2. Figure 2A shows the entire structure of the pyramidal probe, and Fig. 2B is an enlarged view of the diode structure of the probe indicating that for this probe the opening in the aluminum at the end of the tip is approximately $200\text{ nm} \times 200\text{ nm}$. Probes can be routinely fabricated with aperture sizes ranging from 200 to less than 100 nm , which is a factor-of-5 times smaller than for probes produced previously.⁹ Note that the creation of this small opening is achieved with a batch fabrication process without the use of lithography. With these methods an ultrasharp tip, a small Schottky contact area, and a very small (100 nm) optically sensitive region have been realized. The aluminum contact

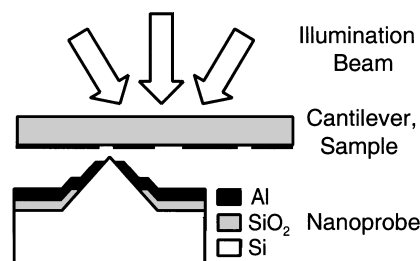


Fig. 1. Schematic of the imaging system, in which non-contact AFM is used for height control. The imaged structure is created on a $2\text{ mm} \times 150\text{ }\mu\text{m} \times 50\text{ }\mu\text{m}$ glass cantilever that is dithered near its resonant frequency. This sample consists of submicrometer holes in a 40-nm aluminum film. The nanoprobe is mounted on a piezoelectric scanning tube. A cut-away schematic of the nanoprobe is shown at the bottom. It consists of a micromachined silicon pyramid with 100-nm silicon dioxide covering all but the last $2\text{ }\mu\text{m}$. In addition, the structure is covered by an 80-nm aluminum film with a small ($100\text{--}200\text{-nm}$) opening in the film at the end of the tip.

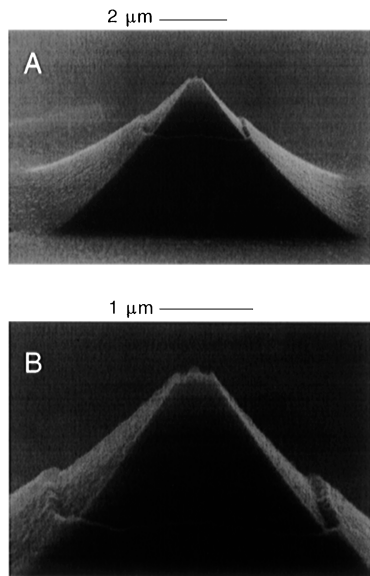


Fig. 2. Scanning-electron-microscopy images of the photodiode nanoprobe at two magnifications: (A) The entire probe structure and (B) an enlarged view of the diode structure. The enlarged view indicates that for this probe the opening in the aluminum is approximately $200 \text{ nm} \times 200 \text{ nm}$ and defines the optically sensitive area of the probe.

near the tip end creates a built-in field that rapidly collects the photogenerated carriers. The aluminum also acts as an aperture that currently defines the spatial resolution of the probe.

Electrical and optical characterization of the photodiode probes was reported previously.⁹ The characterization shows that the diodes have a sensitivity of approximately $150 \text{ fW}/\sqrt{\text{Hz}}$, which is compatible with the achievement of $10 \text{ nm} \times 10 \text{ nm}$ spatial resolution at an illumination intensity of $1 \text{ W}/\text{cm}^2$.

We employed the NPOM probe in high-resolution intensity mapping. The imaging system is illustrated at the top of Fig. 1. The nanoprobe is mounted on a piezoelectric scanning tube, and the sample is located on a cantilever, permitting the use of noncontact atomic-force microscopy (AFM) for height control. Nanometer-scale structure on the sample is created as follows¹¹: A 40-nm aluminum film is deposited on a glass cantilever containing a sparse layer of latex spheres. The latex particles are removed after the aluminum deposition by immersion in an ultrasonic cleaner followed by gentle wiping with an alcohol-wetted tissue. This results in holes in the aluminum film of the size of the latex particles. A He-Ne laser beam that is focused midway down the length of cantilever is used for the noncontact AFM force detection. It was verified that the AFM laser light is not detected by the NPOM probe. The sample is illuminated with a second He-Ne laser beam focused on the back of the film directly over the NPOM probe. The illumination intensity of this beam at the sample surface is $10 \text{ W}/\text{cm}^2$.

Two samples are imaged, the first with 800-nm holes and the second with 200-nm holes. The cantilever is driven near resonance at an amplitude of 20 nm, and the photodiode probe is raster scanned while the AFM

feedback loop keeps it at a constant average distance from the sample surface. The 20-nm cantilever dither produces a small ac modulation of the NPOM signal. The ac signal can be detected by a lock-in amplifier, or the dc component can be measured directly. Simultaneous optical and topographic images are taken.

Images of an 800-nm hole in a 40-nm-thick aluminum film are shown in Fig. 3. The image at the left is a noncontact AFM topographic image, and the image at the right displays the nanoprobe photocurrent detected by the lock-in amplifier at the dither frequency. Below each image is a corresponding line scan cut through the middle of the hole. Since the probe is following the contour of the surface it is essential to verify that the optical information and topographic information are independent, which we do by examining the line scans. The AFM image shows that there is a hemispherical bump nearly filling the bottom of the hole in the aluminum film (most likely contamination), a feature that was not seen in any of the other samples. Whereas the topographic image shows the bump inside the hole, the optical image is approximately uniform across the bottom of the hole, demonstrating that the NPOM probe is not just mapping topography. Also visible in the optical line scan is the sharp transition to a larger optical signal as the probe enters the hole. This transition length is approximately 100 nm.

Images containing several 200-nm holes are shown in Fig. 4. The left image is a topographic image, and the right image is a dc optical image. Below each image is a vertical line cut as indicated in the image. The transition length of the optical signal at the hole edges is approximately 100 nm. The optical image also indicates that the optical intensity outside the hole is not zero but drops off over hundreds of nanometers. Scanning-electron-microscopy images of the detector tip indicate that this slow drop-off is not due to poor resolution of the detector. We can readily see this nonzero optical signal outside the holes by looking at the ac component of the optical signal; the vertical

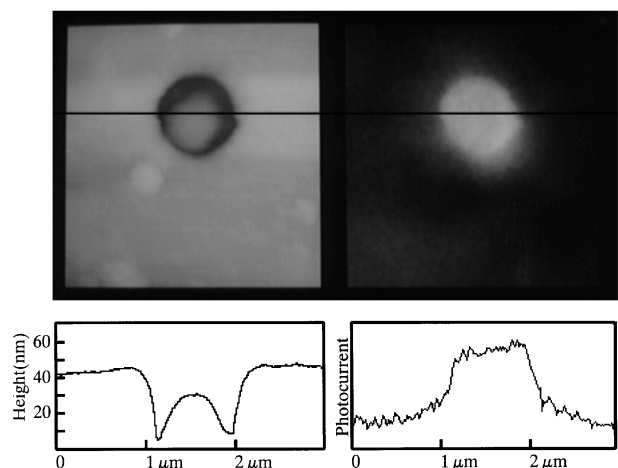


Fig. 3. $3 \mu\text{m} \times 3 \mu\text{m}$ images of an 800-nm hole in a 40-nm-thick aluminum film. The left image is an AFM topographic image; the image at the right shows the ac component of the optical signal. Below each image is a corresponding line scan cut through the middle of the hole.

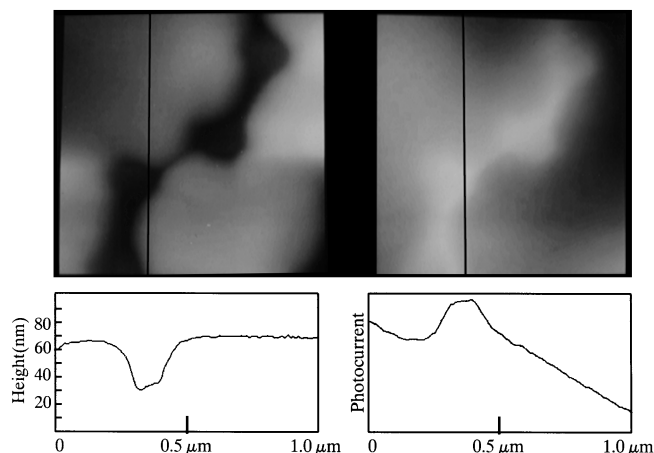


Fig. 4. $1\ \mu\text{m} \times 1\ \mu\text{m}$ images of several 200-nm holes in an aluminum film. The left image is a topographic image; the right image shows the dc component of the optical signal. Below each image is a vertical line cut as indicated in the image.

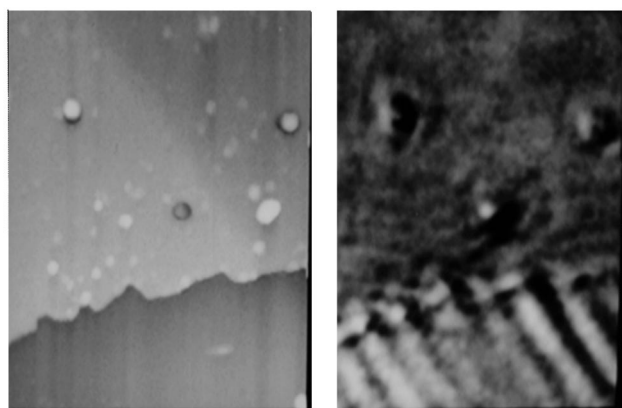


Fig. 5. $11\ \mu\text{m} \times 15\ \mu\text{m}$ images near the edge of an aluminum film, showing interference patterns of the optical fields near a conducting surface. The region at the bottom of the images, below the aluminum edge, is transparent glass. The left image is topography; the right image is the ac optical signal at the modulation frequency and corresponds to the vertical derivative of the optical intensity.

dither tends to accentuate variations of intensity on the slowly varying background.

Figure 5 shows $11\ \mu\text{m} \times 15\ \mu\text{m}$ images near an edge of the aluminum film. The film contains several 800-nm holes and some latex particles that were not removed by the cleaning. The region at the bottom of the images, below the aluminum edge, is transparent glass. The left image is topography; the image at the right is the ac optical signal at the dither frequency. This signal corresponds to the vertical derivative of the optical intensity. Optical interference patterns are seen parallel to the aluminum edge to a distance of $4\ \mu\text{m}$ from the edge and are also seen radially surrounding the holes in the film to a distance of approximately $1\ \mu\text{m}$. These patterns are believed to be due to light waves scattered across the metal surface from the aluminum edges, and to our knowledge this has not been observed with standard near-field scanning optical mi-

croscopy. The spatial variations in the optical intensity in the glass region correspond to interference effects in the illumination beam.

The nanoprobe is also sensitive to temperature and may be an effective tool for high-resolution thermal microscopy.¹² In principle, direct optical heating of the aluminum films could provide a thermal contribution to the nanoprobe signal; however, our data indicate that any thermal contribution to the signal is small compared with the optical contribution. This can be readily seen from Fig. 4—if the thermal contribution were dominant, the nanoprobe signal would be smaller rather than larger over the holes in the aluminum. The previously published spectral response of an illuminated nanoprobe also shows that its signal is dominated by the optical response of silicon.

In summary, a new near-field optical microscopy technique with edge response of the order of 100 nm has been demonstrated. Photodiode probes with $100\ \text{nm} \times 100\ \text{nm}$ optically sensitive areas have been constructed for NPOM by use of batch fabrication methods. Simultaneous noncontact AFM topographic and near-field optical imaging of 800- and 200-nm holes in aluminum films has been performed with the probes. The nanoprobe has been used to measure small differential changes in the optical intensity near a conducting surface showing interference patterns created by the surface boundaries. The photodiodes have a $150\text{-fW}/\sqrt{\text{Hz}}$ detection sensitivity. With this level of sensitivity the probes may be useful for performing optical spectroscopy for chemical identification.

We thank ICM, Ltd., Prague, Czech Republic, and HEDCO Microelectronics Laboratory, University of Utah, for providing fabrication facilities. We also thank Robert Huber and Danka Petelenz for helpful discussions regarding the design and fabrication of the nanoprobe. This study was supported by the National Science Foundation (grant ECS-9212407).

References

1. E. Betzig and J. K. Trautman, *Science* **257**, 189 (1992).
2. H. F. Hess, E. Betzig, T. D. Harris, L. N. Pfeiffer, and K. W. West, *Science* **264**, 1740 (1994).
3. J. K. Trautman, J. J. Macklin, L. E. Brus, and E. Betzig, *Nature (London)* **369**, 40 (1994).
4. F. Zenhausen, M. P. O'Boyle, and H. K. Wickramasinghe, *Appl. Phys. Lett.* **65**, 1623 (1994).
5. D. R. Busath, R. C. Davis, and C. C. Williams, *Proc. SPIE* **1855**, 75 (1993).
6. H. U. Danzebrink and U. C. Fischer, in *Near Field Optics*, D. W. Pohl and D. Courjon, eds. (Kluwer, Dordrecht, The Netherlands, 1993), pp. 303–308.
7. D. R. Busath, "Near-field photodetection probe for near-field optical microscopy," M. S. thesis (University of Utah, Salt Lake City, Utah, 1994).
8. H.-U. Danzebrink, *J. Microsc.* **167**, 276 (1994).
9. R. C. Davis, C. C. Williams, and P. Neuzil, *Appl. Phys. Lett.* **66**, 2309 (1995).
10. G. Kolb, K. Karrai, and G. Abstreiter, *Appl. Phys. Lett.* **65**, 3090 (1994).
11. K. Lieberman and A. Lewis, *Appl. Phys. Lett.* **62**, 1335 (1993).
12. C. C. Williams and H. K. Wickramasinghe, *Appl. Phys. Lett.* **49**, 1587 (1986).